Attitude Stabilization of a Biologically Inspired Robotic Housefly via Dynamic Multimodal Attitude Estimation

Domenico Campolo[1], Giovanni Barbera[2] Luca Schenato[2], Lijuan Pi[3], Xinyan Deng[3] Eugenio Guglielmelli[1]

[1] *Biomedical Robotics Laboratory of the Campus Bio-Medico University, 00128 Roma - Italy*

[2] *Department of Information Engineering of the University of Padova, 35131 Padova - Italy*

[3] *Department of Mechanical Engineering, University of Delaware, Newark, DE - USA*

campolo@sssup.it

Abstract

In this paper, we study sensor fusion for the attitude stabilization of Micro Aerial Vehicles (MAVs), in particular mechanical flying insects. Following a geometric approach, a dynamic observer is proposed which estimates attitude based on kinematic data available from different and redundant bio-inspired sensors such as halteres, ocelli, gravitometers, magnetic compass and light polarization compass. In particular, the traditional structure of complementary filters, suitable for multiple sensor fusion, is specialized to the Lie group of rigid body rotations SO(3). The filter performance based on a 3-axis accelerometer and a 3-axis gyroscope is experimentally tested on a 2 degrees-of-freedom support showing its effectiveness. Finally, attitude stabilization is proposed based on a feedback scheme with dynamic estimation of the state, namely the orientation and the angular velocity. Almost-global stability of the proposed controller in the case of dynamic state estimation is demonstrated via the separation principle, and realistic numerical simulations with noisy sensors and external disturbances are provided to validate the proposed control scheme.

keywords: attitude control on SO(3), separation principle, geometric control, complementary filtering, biologically inspired robots.

1 Introduction

The development of Unmanned Air Vehicles, (UAV), has been a very active area of research for both civil and military applications. Many remarkable achievements have been obtained with large fixed and rotary aircrafts, however their use in many tasks is limited by their maneuverability and size. In order to overcome these limitations, the extraordinary flight capabilities of insects have inspired the design of small Micro Aerial Vehicles (MAVs) and in particular of inch size robots with flapping wings mimicking real flying insects [1]. Their unmatched maneuverability, low fabrication cost and small size

make them very attractive for cost-critical missions in environments which are impenetrable for larger size UAVs such as helicopters or airplanes. Moreover, the latest progresses in insect flight aerodynamics [2] and in micro-technology [3] are providing sufficient tools to fabricate flying insect micro-robots, as shown by the recent take-off of flapping flight robotic insect [4]. Although many problems remain to be solved in terms of fabrication and electromechanical design, the next fundamental challenge to be undertaken is the design of control architectures and algorithms to control and navigate flapping flight robotic insects. It has been observed by biologists that insects can control the generation of forces and torques by modulating the wing kinematics trajectories [2] [5]. This observation has suggested the use of averaging theory tools and a bio-inspired parameterization of the wing kinematics to decouple the wing control design from the attitude control design [7] [8]. This approach has been shown successful also in other bio-mimetic forms of locomotion such as fish swimming [6], and greatly simplifies the design of an autonomous navigation systems, since it naturally leads to a hierarchical architectures [8].

Based on these considerations, in this paper, we focus on the design of attitude control which uses as inputs the signals coming from bio- inspired sensors such as ocelli, halteres, magnetometers and gravitometers. The ability of controlling attitude in a robust and stable manner is fundamental for the design of path planning and navigation control schemes. Previous work exists in this context. For instance, in [9] the authors propose a static output feedback scheme for hovering recovery, however this scheme is sensitive to measurement noise and external disturbances, moreover cannot be easily extended to attitude maneuvering or control schemes based on body orientation. Rifai *et al.* [10] provide an attitude control scheme which takes into account saturation limits, but they do not consider sensors and assume to have access to exact body orientation and angular velocity. Finally, Epstein *et al.* [11] propose a dynamic output feedback schemes based on a linearized model of the insect dynamics suitable for longitudinal control or other simple flight modes, but not for more aggressive maneuvers. Here, we propose a *dynamic* output feedback control scheme that is globally stable and that is based on state estimation from redundant measurements, make it more robust to external disturbances and measurement noise. In particular, we show that we can decouple the orientation estimation problem from the attitude control problem. Although, this separation principle is classical for linear dynamical systems, it is hard to be guaranteed for general nonlinear systems and in particular for the Lie group of rigid body orientations $SO(3)$. Although this scheme has been specifically designed for robotic flying insects with bio-inspired sensors, it is rather general and can be used also for more traditional UAVs as long as the output signals are "linear" in the rotation matrix, as explained later. In fact, this scheme has the advantage to be globally stable differently from more traditional control strategies based on Extended Kalman Filters.

As for the outline of the paper, Section 3 briefly describes the attitude dynamics of a robotic flying insect and reviews navigation sensory system of real insects. Section 4 presents a complementary filter for sensor fusion as well as the experimental validation of its performance. Section 5 proposes a control feedback based on the dynamic attitude estimation which is proven to be globally stable via the separation principle, and it is tested using realistic numerical simulations. Before proceeding some

mathematical background is presented.

2 Mathematical Background

This section briefly describes the notation and several geometric notions that will be used throughout the paper. For additional details, the reader is referred to texts such as [12, 13, 14, 15, 16].

2.1 Basic Definitions

As shown in [12, 13], the natural configuration space for a rigid body is the *Lie group* $SO(3)$, i.e. the configuration of a rigid body can always be represented by a rotation matrix R, i.e. a matrix such that $R^{-1} = R^T$ and $\det R = +1$.
Consider now the coordinate frames $\mathbb{R}^3_S$ and $\mathbb{R}^3_B$:

- $\mathbb{R}^3_S \approx \mathbb{R}^3$: the *space* coordinate frame, or initial configuration frame.
- $\mathbb{R}^3_B \approx \mathbb{R}^3$: the *body* frame, which is attached to the body (can be thought of as defined by the sensors sensitive axis), initially coincident with the space frame.

An element R of $SO(3)$ can be thought of as a map from the body frame to the space frame, i.e. $R : \mathbb{R}^3_B \to \mathbb{R}^3_S$.

A trajectory of the rigid body is curve $R(t) : \mathbb{R} \to SO(3)$. The velocity vector $\dot{R}$ is tangent to the group $SO(3)$ in R but, as shown in [12, 13], rather than considering $\dot{R}$, two important quantities are worth to be considered:

- $\dot{R}\,R^T$: representing the rigid body angular velocity relative to the space frame;
- $R^T\dot{R}$: representing the rigid body angular velocity relative to the body frame.

These are both elements of the *Lie algebra* $so(3)$, i.e. the tangent space to the group $SO(3)$ at the identity I.

Elements of the Lie algebra are represented by skew-symmetric matrices. Systems on Lie groups described in terms of body (space) coordinates are called *left-invariant* (*right-invariant*).
Left-invariance: let $R_1(t)$ be a trajectory of a rigid body relative to a space frame $\mathbb{R}^3_{S_1}$. Consider a change of space frame $G : \mathbb{R}^3_{S1} \to \mathbb{R}^3_{S2}$, now $R_2(t) = GR_1(t)$ represents the *same* trajectory but with respect to the new space frame. It is straightforward to verify that $R_2^T\dot{R}_2 = R_1^T\dot{R}_1$, i.e. the angular velocity relative to the body frame $R^T\dot{R}$ does not depend on the choice of space frame.
Right-invariance: similarly, it can be shown that the angular velocity of a rigid body relative to a space frame $\dot{R}\,R^T$ does not depend on the choice of coordinate frame attached to the body.

In the case of $SO(3)$, there exists [13] an isomorphism of vector spaces $\widehat{\cdot}: so(3) \to \mathbb{R}^3$, referred to as *hat* operator, that allows writing $so(3) \approx \mathbb{R}^3$. For a given vector $a = [a_1\ a_2\ a_3]^T \in \mathbb{R}^3$, we write:

$$\widehat{\cdot}: a = \begin{bmatrix} a_1 \\ a_2 \\ a_3 \end{bmatrix} \longrightarrow \begin{bmatrix} 0 & -a_3 & a_2 \\ a_3 & 0 & -a_1 \\ -a_2 & a_1 & 0 \end{bmatrix} = \widehat{a} \tag{1}$$

Denote $(\cdot)^\vee : \mathbb{R}^3 \to so(3)$ its inverse, referred to as *vee* operator:

$$(\cdot)^\vee : \widehat{a} = \begin{bmatrix} 0 & -a_3 & a_2 \\ a_3 & 0 & -a_1 \\ -a_2 & a_1 & 0 \end{bmatrix} \longrightarrow \begin{bmatrix} a_1 \\ a_2 \\ a_3 \end{bmatrix} = (\widehat{a})^\vee \tag{2}$$

The Lie algebra is equipped with an operator, the *Lie brackets* $[\cdot, \cdot]$ which is defined by the matrix commutator:

$$[\widehat{a}, \widehat{c}] = \widehat{a}\,\widehat{c} - \widehat{c}\,\widehat{a} = \widehat{a \times c} \tag{3}$$

where $a, c \in \mathbb{R}^3$, $\widehat{a}, \widehat{c} \in so(3)$ and $\times$ is cross product in $\mathbb{R}^3$.

Given a finite-dimensional vector space V, let V^* be its *dual* space, i.e. the space whose elements (*covectors*) are linear functions from V to $\mathbb{R}$. If $\sigma \in V^*$, then $\sigma : V \to \mathbb{R}$. Denote the value of σ on $v \in V$ by $\langle \sigma, v \rangle$, i.e. the *pairing* operator $\langle \cdot, \cdot \rangle : V^* \times V \to \mathbb{R}$.

If $V = \mathbb{R}^n$ then $V^* \simeq \mathbb{R}^n$. For all $v \in V$ and $\sigma \in V^* \simeq R^n$ then

$$\begin{array}{rcl} \langle \sigma, v \rangle & = & \sigma^T a \\ \langle\, \widehat{\sigma}, \widehat{v}\, \rangle & = & \frac{1}{2}\mathtt{trace}(\, \widehat{\sigma}^T \widehat{v}\,) \end{array} \tag{4}$$

2.2 Metric properties of $SO(3)$

In what follows necessary background and geometric tools are reviewed in order to define a norm (a distance) on $SO(3)$. This will be used later to prove convergence of the proposed feedback.

On a general manifold M, a positive definite quadratic form $\langle\langle \xi_1, \xi_2 \rangle\rangle_{T_x M}$ defined on any tangent space $T_x M \ni \xi_1, \xi_2$ (the space tangent to M in $x \in M$) is called a *Riemannian metric* [12]. It is the equivalent of the scalar product in $\mathbb{R}^n$, can be used to measure the distance between different points of a manifold, in mechanics a metric is tightly linked to the definition of kinetic energy [16]. A metric is extra structure, does not come with the manifold. Many different metrics, i.e. many different distance measures, can be defined on the same manifold [12].

Lie groups are, by definition, manifolds and therefore are entitled to posses metric properties. Lie groups, in particular $SO(3)$, are structured in such a way that some metrics *naturally*[1] arise. A *left-invariant* metrics does not depend on the choice of the space frame, i.e. it only needs to be defined on the Lie algebra and then it can be left-translated to the tangent space at any other group element:

$$\langle\langle R\,\widehat{a}, R\,\widehat{c} \rangle\rangle_{T_R SO(3)} = \langle\langle \widehat{a}, \widehat{c} \rangle\rangle_{so(3)}$$

[1] *Natural* means that it does not depend on a particular choice of coordinates.

where $R \in SO(3)$ and $\widehat{a}, \widehat{c} \in so(3)$.

Still, there many choices for a metric in the Lie algebra, as many as there are positive definite matrices P:

$$\langle\langle \widehat{a}, \widehat{c} \rangle\rangle_{so(3)} \triangleq a^T P\, c$$

where $a, c \in \mathbb{R}^3$ correspond to $\widehat{a}, \widehat{c} \in so(3)$ as in Eq.(1). However, there only exists one choice (up to a coefficient, [12, 13, 16, 17]) when the metrics needs to be *bi-invariant* (i.e. both right- and left-invariant):

$$\langle\langle \widehat{a}, \widehat{c} \rangle\rangle_{so(3)} \triangleq a^T I\, c = a^T\, c = \langle a, c \rangle \tag{5}$$

where I is the 3×3 identity matrix.

Two main results provided in [17] are:

- the existence of a natural norm[2] on $SO(3)$:

$$\|R\|_{SO(3)} = \langle\langle \widehat{\phi}_R, \widehat{\phi}_R \rangle\rangle^{1/2}_{so(3)} = \|\phi_R\|_{\mathbb{R}^3} \tag{6}$$

- and a formula for computing its time derivative on the Lie algebra $so(3)$:

$$\frac{1}{2}\frac{d}{dt}\|R(t)\|_{SO(3)} = \langle\langle \widehat{\phi}_R, R^T \dot{R} \rangle\rangle_{so(3)} R^T >_{so(3)} \tag{7}$$

where $\widehat{\phi}_R \in so(3)$, also referred to as $\log R$, is defined as the angular velocity that takes the rigid body from I to $R \in SO(3)$ in *one* time unit, see [13] for details on the *logarithmic map*:

$$\widehat{\phi}_R = \log R = \frac{\theta_R}{2 \sin \theta_R}(R - R^T) \tag{8}$$

where, for $\texttt{trace}(R) \neq -1$, θ_R satisfies $1 + 2\cos\theta_R = \texttt{trace}(R)$ and $\|\phi_R\|^2 = \theta_R^2$, and the *Rodrigues' formula*:

$$R = \exp(\widehat{\phi}_R) = I + \alpha_R\, \widehat{\phi}_R + \beta_R\, \widehat{\phi}_R^2 \tag{9}$$

where $\alpha_R = \|\phi_R\|^{-1} \sin\|\phi_R\|$ and $\beta_R = (1 - \cos\|\phi_R\|)\|\phi_R\|^{-2}$.

3 BIOLOGICALLY INSPIRED ROBOTIC HOUSEFLY

In this section we review the most important features of a Micromechanical Flying Insect, summarizing some of the results presented in [7][8].

3.1 Dynamics of the Micromechanical Flying insect

Insect flight dynamics is still a very active area of research. In particular, there is great interest in understanding the unsteady state nature of flapping wings aerodynamics, which is believed to be source of the high maneuverability of insect flight as compared to fixed-winged vehicles and helicopters [18]. A

[2] Which measures the distance between R and the identity I.

detailed discussion of flying insect aerodynamics and modeling is beyond the scope of this paper, and we address the interested readers to the recent paper by Deng *et al.* and references therein [7]. Here, we simply summarize some results relevant to our discussion on attitude stabilization.

Since the mass of the wings is negligible with respect to the body mass, the dynamics of a flying insect can be modeled as the dynamics of a rigid body subject to external forces and torques. In particular, as long as attitude is concerned, the dynamics is described by:

$$J\dot{\omega} \quad = \quad \tau_{aero} - \omega \times J\omega \tag{10}$$

where J is the moment of inertia of the insect, τ_{aero} is the total external torque with respect to the insect center of mass in the body frame due to the aerodynamic forces generated by the flapping wings, and ω is the angular velocity with respect to the body.

The dynamics of (10), affine with respect to the forcing input τ_{aero}, can be averaged out as in [8]. The time varying components of the torque can be neglected while the mean value of the torque τ_{FB} will be used as the feedback (FB) term for attitude stabilization. As this term depends upon the current orientation R and the current angular velocity ω, the *averaged* attitude dynamics of a mechanical flying insect are described by the system

$$\begin{cases} \dot{R} = R\widehat{\omega} \\ \dot{\omega} = J^{-1}(J\omega \times \omega + \tau_{FB}(R, \omega)) \end{cases} \tag{11}$$

where the $\widehat{\cdot}$ *hat* operator transforms the ω vector into a skew-symmetric matrix $\widehat{\omega}$ and (R, ω) is an element of $SO(3) \times so(3)$, i.e. the product space of the *Lie Group* $SO(3)$ of rigid body rotations and its *Algebra* $so(3)$.

3.2 The Sensory System of Flying Insects

The highly specialized sensory system of flying insects is at the base of their extraordinary flying performance. In fact flying insects can rely on an heterogeneous set of redundant sensors for controlling flight maneuvers and navigate the environment. Redundancy is the key to robustness. Some of these sensors represent a rich source of inspiration for the design of mechanical flying insects [19][7] and they motivate the control strategy proposed in this work.

3.2.1 Halteres

The halteres are club-shaped small appendages behind each wing that oscillate in anti-phase with respect of the wing, as shown in Fig. 1. The plane of oscillation is slightly tilted toward the tail of the insect to be able to measure Coriolis forces along all three body axes [20]. The halteres function as tiny gyroscopes and through appropriate signal processing [21] they can reconstruct the body angular velocity vector:

$$y_{hl} = \omega \tag{12}$$

Recently, preliminary prototypes of micro-electromechanical halteres have been fabricated and have shown promising results [22].

Figure 1: Photo of a fly haltere.

3.2.2 Mechanoreceptors

Many parts of the insect body such as wings, antennae, neck and legs are innervated by campaniform sensilla. These cells can measure and encode pressure forces when they are stretched or strained [23]. For example sensilla at the base of wing hinges can measure aerodynamic forces, which are used to fine tune the wing motion. Similarly, the sensilla on the legs might be used to measure the gravity sensor, thus acting as a gravitometer. Therefore, in static conditions, insect can measure the gravity vector with respect to the body frame, i.e.

$$y_g = R^T g_0 \tag{13}$$

where g_0 are the (known) gravity vector components, measured with respect to the fixed frame. In non-static conditions, also noninertial accelerations add-up to the output of mechanoreceptors, as a form of disturbance. Combining information from mechanoreceptors and halteres (sensor fusion) can greatly alleviate the effects of such disturbances.

3.2.3 Ocelli

The ocelli are three additional light-sensitive organs located at the vertices of an imaginary triangle on the middle of head of the insect as shown in Fig. 2, and provide signals that are used for stabilization

with respect to rapid perturbations in roll and pitch [19]. In fact, these sensors collect and measure light intensity from a portion of the sky, and they estimate the position of the sun with respect to insect body by comparing the signals from the left and right ocelli to estimate the roll angle, and by comparing the signal from the forward-looking ocellus with the mean of the signals from the left and the right ocelli to estimate the pitch angle [24].

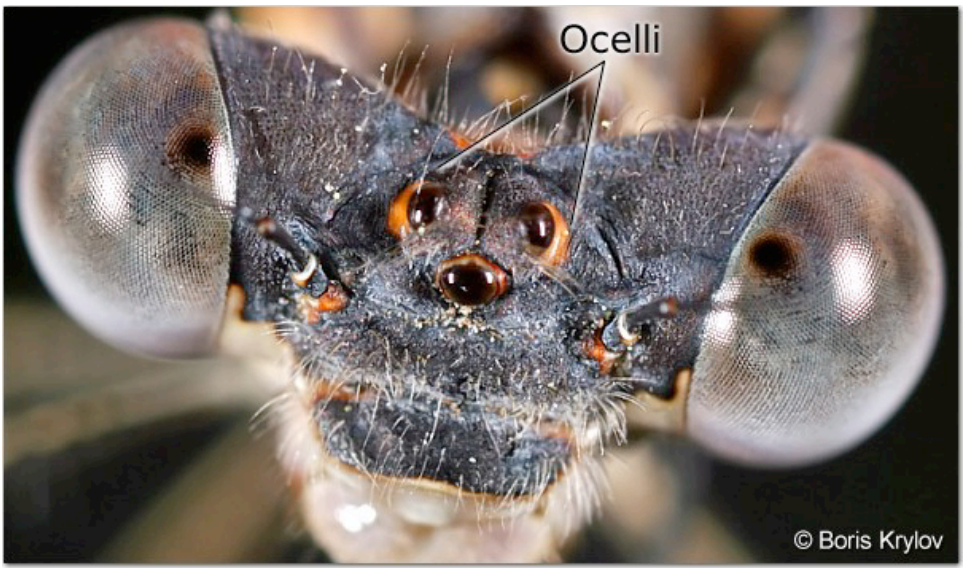

Figure 2: Photo of fly's head showing compound eyes and the ocelli with its three photoreceptors.

3.2.4 Compound eyes

The compound eyes of the insects are an advanced vision system that processes different types of signals needed for the optomotor systems. In fact they can process the visual stimuli to estimates angular velocities thanks to large-field neurons that are tuned to respond to the specific patterns of optic flow that are generated by yaw, roll and pitch [25], as well as body orientation and position by higher level visual processing like object fixation and landmarks detection for navigation and path planning [11]. However, such signals requires quite a specialized signal processing system that might not be necessary for attitude stabilization, which is the objective of this work. However, the dorsally directed (upward-looking) regions of the compound eyes of many insects are equipped with specialized photoreceptors that are sensitive to the polarized light patterns that are created by the sun in the sky. More precisely insects can measure their orientation relative to the direction of the light polarization: $p_0 \in \mathbb{R}^3$, as:

$$y_p = R^T p_0 \tag{14}$$

Differently from the ocelli, the light polarization direction is not affected by light intensity. Bio-inspired polarized light compasses are easier to fabricate that the full insect visual system, and have been successfully fabricated and used for robot navigation [26] and it is relevant to the flight control design proposed in this work.

3.2.5 Magnetic compass

Recent studies indicate that some insects also can detect the earth magnetic and it is used to maintain a desired heading direction [27]. Similarly to the light polarization sensor, we can argue that insect can measure the components of the magnetic field with respect to the body as follows:

$$y_m = R^T b_0 \tag{15}$$

where $b_0 \in \mathbb{R}^3$ is the direction of magnetic field relative to the fixed frame. A possible electromechanical implementation of a magnetic compass suitable for small size vehicles is given in [28].

4 SENSOR FUSION VIA COMPLEMENTARY FILTERS

The sensory system of real insects is clearly redundant, e.g. kinematic quantities such as the angular velocity are derived from more than one sensor. Information from different sensors is then 'fused' together. Complementary filters traditionally arise in applications where redundant measurements of the same signal are available [29] and the problem is combining all available information in order to minimize the instrumentation error.

For sake of simplicity, consider only two sensors, s_1 and s_2, providing readings of the *same* quantity, e.g. the angular velocity ω, with different noise characteristics, i.e. $s_1 = \omega + n_1$ and $s_2 = \omega + n_2$, where $\|n_1\| < \|n_2\|$ at high frequency while $\|n_2\| < \|n_1\|$ at low frequency. Then an low-pass filter $L(s)$ and its complementary high-pass filter $H(s) = 1 - L(s)$ can be used to fuse information

$$s_{fusion} = s_1 H(s) + s_2 L(s) = \omega + n_2 L(s) + n_1(1 - L(s)) \tag{16}$$

from two or more sensors (e.g. halteres, ocelli and compound eyes). The cut-off frequency of the filter $L(s)$ can be chosen so that the spectral content of $n_2 L(s) + n_1(1 - L(s))$ will be less than the spectral content of n_1 or n_2 [29].

The kinematic variable ω is dynamically *unaffected* by the filter. The estimated variable (i.e. the output of the filter) is related to the input variable via a purely algebraic relation in the time domain and no dynamics are involved in the noiseless case. Such filters can be safely used in feedback loops to fuse readings of the *same* kinematic variable from different sensors since no extra dynamics is added to the overall system and stability (which involves noiseless conditions) is not affected.

Complementary filters can be generalized to fuse information deriving from sensors when the sensed variables are related by differential equations, e.g. position and speed. In these cases, the filter introduces some dynamics between the estimated output and the sensed inputs.

The differential equations relating the sensed variables may be nonlinear, this is typically the case when attitude is concerned. Theory of complementary and Kalman filters has been traditionally used to design attitude filters. Although the Kalman filters can be extended (EKF) to nonlinear cases, they fail in capturing the nonlinear structure of the configuration space of problems involving, for example,

rotations of a rigid body, and most importantly, they can run into instabilities. On the other hand, nonlinear filters [30], in particular complementary filters, can better capture such a nonlinear structure.

4.1 Dynamic Attitude Estimation

As an example of use of complementary filters when *different* kinematic variables are involved, consider the linear case of a rotational mechanical system with one degree of freedom (θ). As shown in [29], complementary filters such as the one represented in Fig. 3 are traditionally used to fuse information available from both angular position sensors and tachometers, respectively θ_{sens} and ω_{tacho}. Let θ^* be the estimate of θ. The filter gain k in Fig. 3 determines the transition frequency of the filter after which the data from the tachometer (ω_{tacho}) are weighted more whereas before the transition frequency data from the position sensors (θ_{sens}) are predominant on the dynamic equation (the integrator $1/s$). The optimal value for k is in fact determined from the spectral characteristics of measurement noise [29].

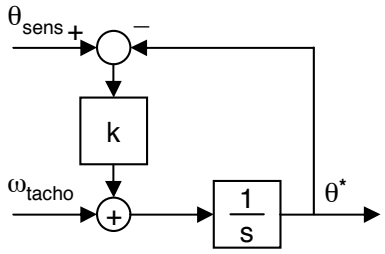

Figure 3: Linear complementary filter for a rotational mechanical system with one degree of freedom.

Differently from previous example, $SO(3)$ is a *nonlinear* space and that is where the advantages of a geometric approach can be fully appreciated. Besides nonlinear dynamics, the very definition of estimation error requires caution. In the linear case $e = \theta - \theta^*$ is a typical choice while quantities such as $R - R^*$ with $R, R^* \in SO(3)$ are no longer guaranteed to belong to $SO(3)$. Following [17], the estimation error will be defined as $E = R^T R^*$.

A complementary filter on $SO(3)$ was presented in [31] for dynamic attitude estimation. Main definition, theorem and related lemmas are reported in Appendix A for convenience, the interested reader can refer to [31] for the proof.

A block diagram of the filter, for the specific case of interest, is shown in Fig. 4. Raw data from gyroscopes (ω_{gyr}), from accelerometers (g) and from magnetometers (b) (i.e. a total of 9 channels) are fused together to provide an estimate of the orientation (R^*). The filter also uses two initial readings g_0 and b_0 respectively from accelerometers and magnetometers. The orientation matrix R^* can be initially set to any appropriate value (e.g the 3×3 identity matrix) in the integration block.

As a final note, in linear cases such as in Fig. 3 all the variables belong to the same space $\mathbb{R}^n$. In the nonlinear filter in Fig. 4, variables in different nodes of the block diagram belong to very different spaces, some linear ($so(3)$) and some nonlinear ($SO(3)$). The adopted geometric approach leads to recognize how sensor fusion *naturally* occurs on the linear space of angular velocities, i.e. the Lie algebra $so(3)$.

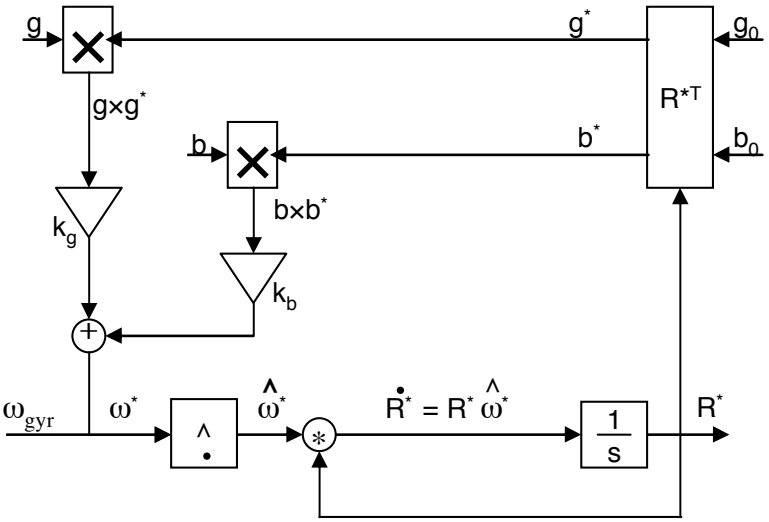

Figure 4: Complementary filter for dynamic attitude estimation.

4.2 Numerical Implementation

The filter in Fig. 4, in principle, can be directly implemented in simulation environments such as MATLAB/ Simulink from MathWorks Inc. Any digital implementation of the filter would *i*) transform the filter in a discrete-time one with time sequence t_n and *ii*) necessarily introduce numerical errors. The main risk is that, as numerical errors accumulate, quantities such as $R^*_n = R^*(t_n)$ are likely to *drift away* from $SO(3)$, i.e. $\det R^*_n$ very different from 1 and/or $R^{*T}_n R^*_n$ very different from the identity matrix I. This can be avoided by considering that data from analog sensors are typically acquired via DACs (Digital to Analog Converters) with a fixed sampling time, let this sampling time be ΔT. In the time interval $t_n \leq t < t_{n+1} = t_n + \Delta T$, data from sensors can be assumed constantly equal to the last sampled value. This allows computing R^*_{n+1} via the Rodrigues' formula [13] as:

$$\begin{aligned} \omega^*_n &= \omega_n + k_g(g_n \times (R^{*T}_n g_0)) + k_b(b_n \times (R^{*T}_n b_0)) \\ \alpha_n &= \sin \|\Delta T \widehat{\omega}^*_n\| \,/\, \|\Delta T \widehat{\omega}^*_n\| \\ \beta_n &= (1 - \cos \|\Delta T \widehat{\omega}^*_n\|) \,/\, \|\Delta T \widehat{\omega}^*_n\|^2 \\ R^*_{n+1} &= R^*_n \left(I + \alpha_n \Delta T \widehat{\omega}^*_n + \beta_n \Delta T^2 \widehat{\omega}^{*2}_n\right) \end{aligned} \tag{17}$$

which is guaranteed *not* to drift away from $SO(3)$.

4.3 Experimental Tests of Attitude Estimation

In this section we present some experimental results relative to attitude estimation based on the complimentary filter given by Equations (17).

4.3.1 Experimental Setup

A circuit board equipped with a pair of IDG-300 dual-axis gyroscopes (InvenSense) and one 3-axis ADXL330 accelerometer (Analog Devices) was mounted on a holder and set free to rotate about the

roll (x) and pitch (y) axis (see Fig. 5). The holder included two MAE-3 US-Digital angular sensors

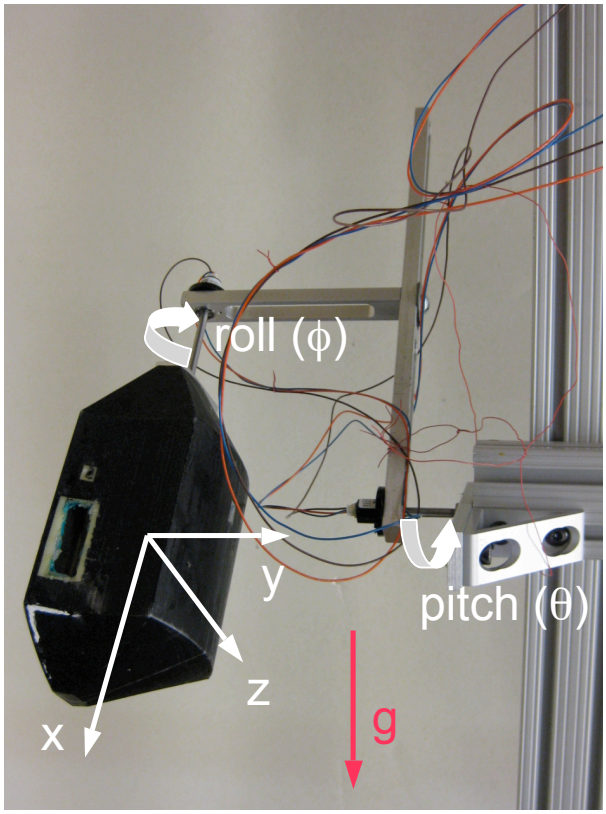

Figure 5: The support used to perform the combined roll/pitch motion. The body-fixed coordinate system is also shown.

to measure exact angular displacement. The accelerometers are used to measure the static gravity acceleration, while the gyroscopes provide the angular rate with respect to the three axes in the body reference frame.

4.3.2 Results

According to the reference frame presented in Fig. 5, and adopting the yaw-pitch-roll Euler angles (ZYX), the rotation matrix $R \in SO(3)$ can be considered as a map from the body-fixed frame to the space frame given by the sequential rotation about the Z_b, Y_b and X_b axis:

$$R = \begin{bmatrix} r_{11} & r_{12} & r_{13} \\ r_{21} & r_{22} & r_{23} \\ r_{31} & r_{32} & r_{33} \end{bmatrix} = R_x(-\phi)R_y(-\theta)R_z(-\psi), \tag{18}$$

being ϕ, θ and ϕ the roll, pitch and yaw angles, respetively. Since this map is surjective, with the only exception of the singularity in $\theta = \pi/2$ for the pitch angle, one can directly evaluate ϕ, θ and ψ invert Eqn. (18), and thus immediately compare the true angular position measured by the position sensors mounted on the holder with the estimated angles from the complimentary filter. Inverting Eqn. (18)

yields

$$\begin{aligned} \theta &= -\arcsin(r_{31}) \\ \phi &= \text{atan2}(\tfrac{r_{32}}{\cos(\theta)}, \tfrac{r_{33}}{\cos(\theta)}) \\ \psi &= \text{atan2}(\tfrac{r_{21}}{\cos(\theta)}, \tfrac{r_{11}}{\cos(\theta)}) \end{aligned} \tag{19}$$

The matrix $R^T(t)R^*(t)$ is guaranteed to converge to the identity matrix I for any initial condition, i.e. the estimated orientation $R^*(t)$ converges to the true orientation $R(t)$, the initial condition of the complementary filter. In the experiments the initial orientation $R^*(t_0)$, was set to be different from the true $R(t_0)$ in order to evaluate the speed of convergence. The results of attitude estimation from the

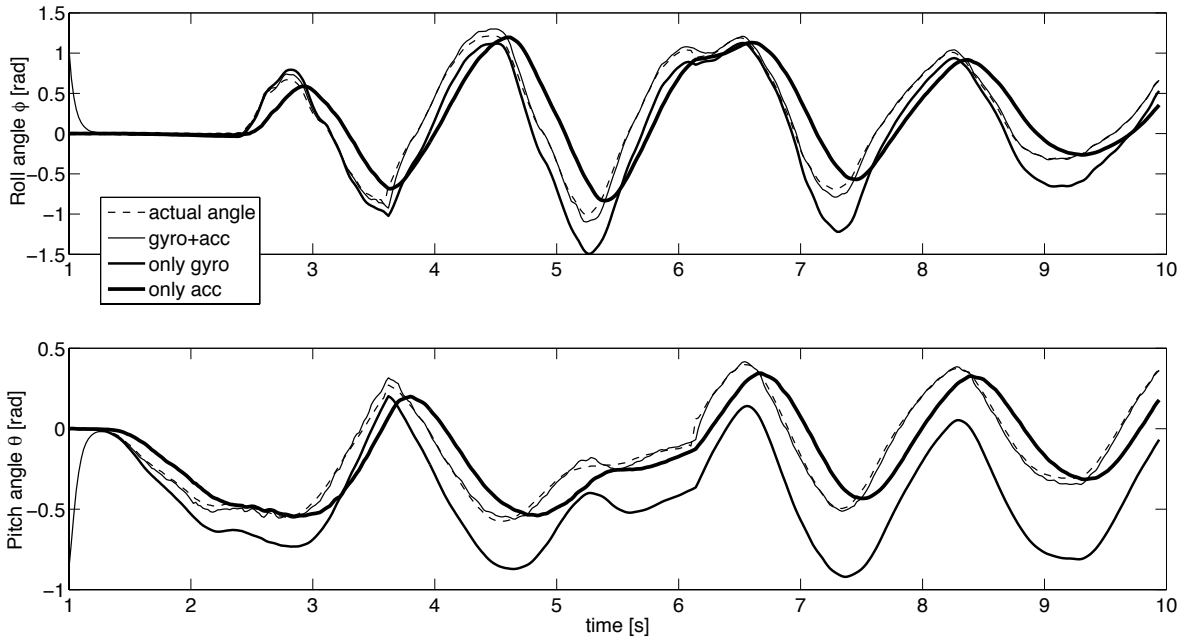

Figure 6: Comparison between the actual roll angle (*top*) and pitch angle (*bottom*) and three different estimations evaluated using the only accelerometers data, the only gyroscopes data or both.

complementary filter using filter gain $k_g = 16$ are shown in Fig. 6 and the associated sensor readouts are shown in Fig. 7 and 8. The plots show rapid convergence of the estimated angles to the true angles in the first half second of the experiments when the body frame is kept fixed, and then they remain very close to the true angles also during the body motion. The effectiveness of sensor fusion is best appreciated by removing either the gyros or the accelerometers from the filter. In the first case, the removal of the gyros results in an evident low pass behavior of the estimated angles which exhibit a time lag as compared to the true angle. Differently, if only gyros are used, the estimated angles have rapid response to body motion, but they incurs in a drift that overtime leads to large offsets as compared to the true angles. The complementary filter, as explained above, fuse the benefits from both sensor modality giving rise to a filter with a very high bandwidth.

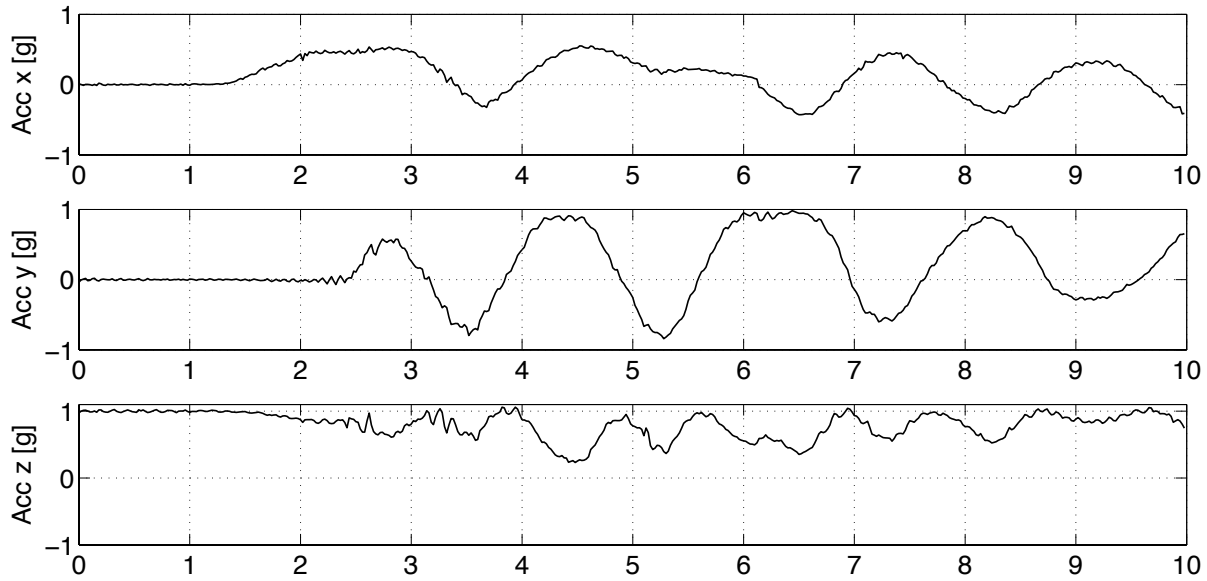

Figure 7: Accelerometers readouts. Readings are normalized with respect to gravity acceleration g.

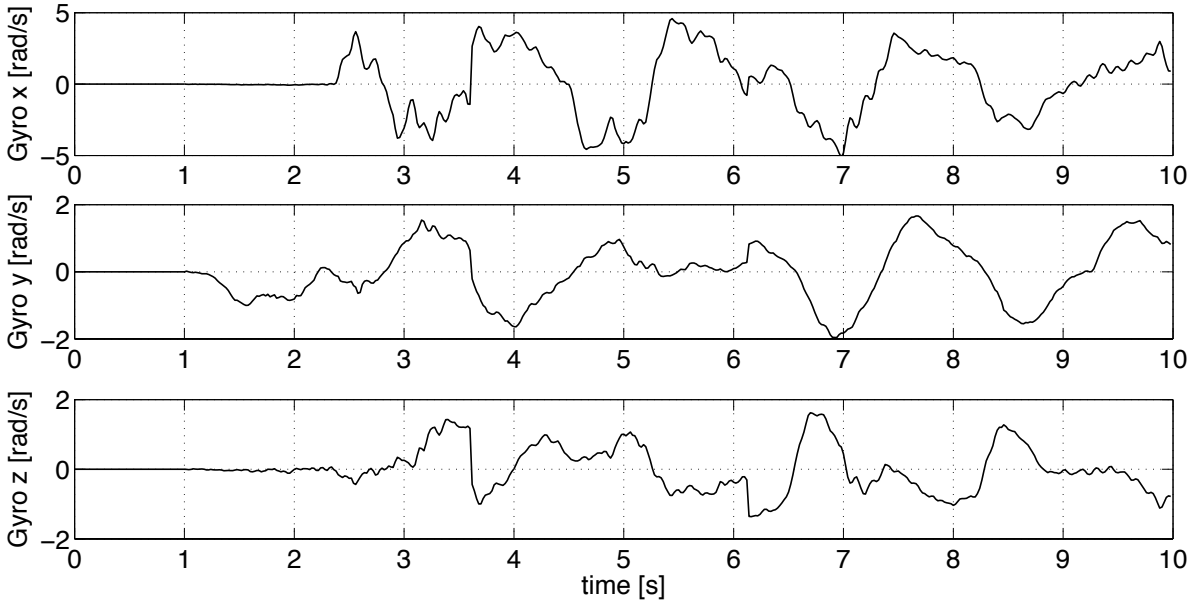

Figure 8: Gyroscopes readouts.

5 ATTITUDE STABILIZATION VIA THE SEPARATION PRINCIPLE

In this section, results of traditional attitude control are first reviewed and then applied to derive a control law based on state feedback. Since in the application of interest the state of the system is not known and only an estimation of the current state can be used as feedback, it is natural to wonder whether dynamic output feedback control preserves the stability properties of the state-feedback control, i.e. whether the *separation principle* holds. Maithripala *et al.* [32, 33] proved that the separation principle also holds in the general case of compact Lie Groups and therefore also for $SO(3)$. For the reader's convenience this general result is restated in terms of $SO(3)$ in the Appendix B. In this section, results from [32, 33] are specialized to $SO(3)$, the Lie Groups of rigid body rotations, and traditional state feedback control is combined with the dynamic attitude observer presented in [31].

5.1 Attitude Control via State Feedback

Traditionally, control of (11) is performed via passivity-based arguments. Maithripala *et al.* [32] show that the system (11) can be stabilized by a state feedback torque $\tau_{FB}(R,\omega)$ which consists of a conservative part, derived from a potential (also referred to as "error") Morse[3] function $U : SO(3) \to \mathbb{R}$, and a dissipative (Rayleigh-type) part:

$$\tau_{FB}(R,\omega) = -J\left(R^T \mathtt{grad}U + k_\omega \widehat{\omega}\right)^\vee \tag{20}$$

where $\mathtt{grad}U$, the *gradient* of the function $U(R)$. Differently from the differential dU, the gradient $\mathtt{grad}U$ depends on the geometry of the space itself. The gradient is in fact defined by the following identities:

$$\begin{aligned} \dot{U}(R) = &\ \langle dU, R\,\widehat{\omega}\rangle \\ = &\ \langle R^T dU, \widehat{\omega}\rangle \\ = &\ \langle\langle R^T \mathtt{grad}U, \widehat{\omega}\rangle\rangle_{so(3)} \end{aligned} \tag{21}$$

where, for a vector space V and its dual V^*, $\langle\cdot,\cdot\rangle : V^* \times V \to \mathbb{R}$ is the *pairing* operator and $\langle\langle\cdot,\cdot\rangle\rangle_V : V \times V \to \mathbb{R}$ is the inner product defined via a proper isomorphism $J : V \to V^*$ as $\langle\langle a,b\rangle\rangle_V = \langle Ja, b\rangle_V$, see [31, 32, 33]. In Mechanics, a *natural* isomorphism J is provided by the inertia tensor (constant in body coordinates) and so the gradient is determined by:

$$R^T \mathtt{grad}U = J^{-1} R^T dU \tag{22}$$

Therefore, the problem of stabilizing (11) is reduced to defining a potential function $U(R)$ on $SO(3)$ with a nondegenerate critical point in the desired configuration $\bar{R} \in SO(3)$. To this end, a commonly used potential function, first introduced by Koditschek in [34], on $SO(3)$ is:

$$U(R) \triangleq \frac{1}{2}\mathtt{trace}(K(I - \bar{R}^T R)) \tag{23}$$

[3] A Morse function is function whose critical points are non-degenerate [16].

where K is a symmetric 3×3 matrix with eigenvalues $\{k_1, k_2, k_3\}$. Once the potential function $U(R)$ is defined, the gradient (and therefore the feedback torque) can be computed as in [35] via the time derivative of the error function:

$$\begin{aligned} \dot{U}(R) = & \ \tfrac{1}{2}\mathtt{trace}(K(-\bar{R}^T\dot{R})) \\ = & \ \tfrac{1}{2}\mathtt{trace}(-K\bar{R}^T R\widehat{\omega}) \\ = & \ \tfrac{1}{2}\mathtt{trace}(\mathtt{skew}(K\bar{R}^T R)^T\widehat{\omega}) \\ = & \ \langle \mathtt{skew}(K\bar{R}^T R), \widehat{\omega}\rangle \end{aligned} \tag{24}$$

where $\mathtt{skew}(A) = \frac{1}{2}(A - A^T)$. This allows computing $R^T\mathtt{grad}U$ from (22):

$$R^T\mathtt{grad}U = J^{-1}\mathtt{skew}(K\bar{R}^T R) \tag{25}$$

Convergence properties of systems like (11) when the state feedback (20) is used can be found in [32, 33], here briefly restated for the case of interest. The proof is based on La Salle's principle [15] and involves a function $V = U(R) + \frac{1}{2}\langle\langle\widehat{\omega}, \widehat{\omega}\rangle\rangle_{so(3)}$as well as a set $S \subset SO(3) \times so(3)$ defined as $S = \{(R, \omega)|\dot{V} = 0\}$.

The sign of $\dot{V}$ is studied as follows:

$$\begin{aligned} \dot{V} & = \dot{U}(R) + \tfrac{1}{2}\dot{\omega}^T J\omega + \tfrac{1}{2}\omega^T J\dot{\omega} \\ & = \dot{U}(R) + \omega^T J\dot{\omega} \\ & = \dot{U}(R) + \omega^T(J\omega \times \omega + \tau_{FB}) \\ & = \dot{U}(R) + \omega^T\tau_{FB} \\ & = \dot{U}(R) + \langle\langle J^{-1}\widehat{\tau}_{FB}, \widehat{\omega}\rangle\rangle_{so(3)} \end{aligned} \tag{26}$$

since $\omega^T(J\omega \times \omega) = 0$ for all $\omega \in \mathbb{R}^3$.

Considering (22) and (20), then:

$$\begin{aligned} \dot{V} = & \ \langle\langle R^T\mathtt{grad}U, \widehat{\omega}\rangle\rangle_{so(3)} + \langle\langle J^{-1}\widehat{\tau}_{FB}, \widehat{\omega}\rangle\rangle_{so(3)} \\ = & \ -k_\omega\|\omega\|^2 \end{aligned} \tag{27}$$

which implies $S = \{(R, \omega)|\omega = 0\}$ and

$$\langle\langle R^T\mathtt{grad}U, \widehat{\omega}\rangle\rangle_{so(3)} + \langle\langle J^{-1}\tau_{FB}, \widehat{\omega}\rangle\rangle_{so(3)} \leq 0 \tag{28}$$

where the inequality is *strict* for all $(R, \omega) \notin S$, implying *asymptotic* convergence. This satisfies the assumption A.1 of Lemma 3 in Appendix B.

In order to perform attitude stabilization of the system (11) via state feedback (20), the current attitude R and angular velocity ω need to be available.

Angular velocity can be directly measured from gyroscopes (for example fusing signals from halteres, ocelli and compound eyes) while attitude can be estimated from mechanoreceptors and magnetic compass sensors, as shown next.

5.2 Dynamic Attitude Estimation Feedback

In this section, previous results on attitude control via state feedback and the dynamic attitude observer are coupled via the separation principle, restated in Appendix B.

The full dynamic equations for the proposed attitude stabilization system are:

$$\begin{cases} \dot{R} = R\,\widehat{\omega} \\ \dot{\omega} = J^{-1}(\tau_{FB}(R^*, \omega^*) - \omega \times J\omega) \end{cases} \quad \textit{attitude controller}$$
$$\begin{cases} \dot{R}^* = R^*\,\widehat{\omega}^* \\ \omega^* = \omega_{gyr} + k_b(b \times b^*) + k_g(g \times g^*) \end{cases} \quad \textit{dynamic observer} \tag{29}$$

The first two equations represent the system dynamics (11) with a feedback τ_{FB} similar to (20) except that it is based on the estimates (R^* and ω^*) of the current orientation and angular velocity, instead of the actual values (R and ω). The last two equations represent the dynamics of the observer (A-5) in Appendix A where, without loss of generality, only the minimum number of independent fields (b and g) is used.

Besides proving almost-global asymptotic stability of the proposed observer, Theorem 1 in [31] (reported in Appendix A) also provides an upper bound of the attitude estimation error E, defined as:

$$E = R^T R^* \tag{30}$$

based on the natural Lyapunov function [17] of the estimation error:

$$W(E) = \frac{1}{2}\|E\|^2_{SO(3)} = \frac{1}{2}\|\phi_E\|^2 \tag{31}$$

where ϕ_E is defined via the logarithmic map as $\widehat{\phi}_E = \log E$.

One of the outcomes of Theorem 1 in [31] is the existence of real number $\eta > 0$ such that, if the initial estimation error $E(0)$ is such that $\texttt{trace}E \neq -1$ (i.e. $\|\phi_E\| < \pi$ which is *almost* globally verified, see Remark 1 below), then a bound for the Lyapunov function is

$$0 < W(E) < W(E(0))\, e^{-\eta t}$$

for all $t > 0$. This translates, via the (31), into an upper bound for the attitude tracking error:

$$\|\phi_E\| < c\|\phi_E(0)\|e^{-\lambda t} \tag{32}$$

where $c = W(E(0))/\|\phi_E(0)\|$ and $\lambda = \eta/2$. This satisfies assumption A.2 of Lemma 3 in the appendix.

In order to apply the separation principle, rewrite (29) as

$$\begin{cases} \dot{R} = R\,\widehat{\omega} \\ \dot{\omega} = J^{-1}(\tau_{FB}(R, \omega) - \omega \times J\omega) + \psi(R, \omega, q) \\ \dot{R}^* = R^*\,\widehat{\omega}^* \\ \omega^* = \omega_{gyr} + k_b(b \times b^*) + k_g(g \times g^*) \end{cases} \tag{33}$$

where $\psi(R, \omega, q)$ represents the term $J^{-1}(\tau_{FB}(R^*, \omega^*) - \tau_{FB}(R, \omega))$. This is possible because ω^* is a (linear) function of R, ω and R^*; R^* can in turn be written as $RR^T R^* = RE$ and E is parameterized by $q \triangleq \phi_E$.

Since $\phi(R, \omega, q)$ is linear in ω and $SO(3)$ is a *compact* Lie group, then assumption A.3 of Lemma 3 in the appendix is also automatically satisfied, see [33, Assumption 3] for details. Recalling that also assumptions A.1 and A.2 in Lemma 3 where satisfied (respectively in (28) and (32)), then Lemma 3 guarantees that the system (29) *almost globally* stabilizes the attitude at $(\bar{R}, 0) \in SO(3) \times so(3)$ and that convergence is *asymptotic*.

Remark 1 (π-rotations) *The chosen Lyapunov function (31) proves convergence* almost *for all possible initial estimation errors $E(0)$. A question arises:* what can be said about the initial configurations which are left out? *Note first that, as clear from the definition of the logarithmic map,* any *configuration can be reached via a rotation about some axis by an angle less than or equal to π. The only configurations left out by the chosen Lyapunov function are those such that* $\texttt{trace}(E) \neq -1$*, i.e. such that $\|\phi_E\| = \pi$. Such configurations correspond to the set of rotations about an arbitrary axis by an angle exactly equal to π and will be referred to as π-rotations.*

The presence of unstable equilibria is inherently related to π- rotations. As a simple example, for the needle of a magnetic compass, the North direction is a stable equilibrium while the South direction (a π-rotation from the North) is an unstable one. In practice, due to the presence of noise, unstable equilibria are not an issue.

5.3 Simulation results

The housefly body is modeled as an ellipsoid with mass $m = 1$ [g] and moment of inertia $J = \text{diag}\{J_x, J_y, J_z\}$, where $J_x = J_y = 1.5 \cdot 10^{-8}$ [kg m^2] and $J_z = 2.5 \cdot 10^{-8}$ [kg m^2]. Three independent sensors are considered for the attitude estimation: a 3-axis gravitomer which measures the gravity vector[4] components with respect to the body frame, a 3-axis magnetometer which measures the geomagnetic field vector[5], and a 3-axis gyroscope with measures the angular velocity vector. Readouts from the gravitometer, the magnetometer and gyroscope are simulated as follows:

$$\begin{aligned} \omega_{gyro} &= \omega(t) + w_1(t) \\ g_{meas}(t) &= P(s)R^T(t)b_0 + w_2(t) \\ b_{meas}(t) &= R^T(t-\tau)g_0 + w_3(t) \end{aligned} \tag{34}$$

where $\omega(t)$ and $R(t)$ obey to Eqn. (29), $w_i(t) \in \mathbb{R}^3$ are zero-mean independent additive gaussian noises with variance $\sigma_1 = 0.4\,[(\text{rad/s})^2], \sigma_2 = \sigma_3 = 0.4$. With a little abuse of notation we indicate with $z(t) = P(s)y(t)$ the filtered version of the signal $y(t)$ where $P(s)$ is the transfer function of a second order low-pass filter which models the dynamics of the accelerometers inside the gravitometer. The variable τ

[4] normalized without loss of generality to $g_0 = [0\ 0\ 1]^T$ with respect to a right-handed space frame

[5] normalized w.l.o.g. to $b_0 = [1\ 0\ 0]^T$

represents a delay in the magnetic sensor outputs which models possible HW/SW measurement signal processing time. In the simulations we used $P(s) = \frac{\omega_n^2}{s^2+2\xi\omega_n s+\omega_n^2}$, where $\omega_n = ??, \xi = 0.7$, and $\tau = 30\,\text{ms}$. The control torque $\tau_{FB}(R^*, \omega^*)$ used in Eqn. (33) was designed based on Eqn. (20) where $k_\omega = 8$ and $K = 30I$. The gains for the filter are set to $k_g = 8, k_b = 13$.

Some closed loop simulations results shown in Fig. 10. During the simulation the body, starting from an orientation $R(0) \neq I \in \mathbb{R}^{3\times3}$, namely $\phi_0 = \theta_0 = \psi_0 = \pi/4$, is driven by the control torque to the desired position $\overline{R}(t) = I$. A block diagram illustrating the control algorithm[6] is presented in Fig. 9.

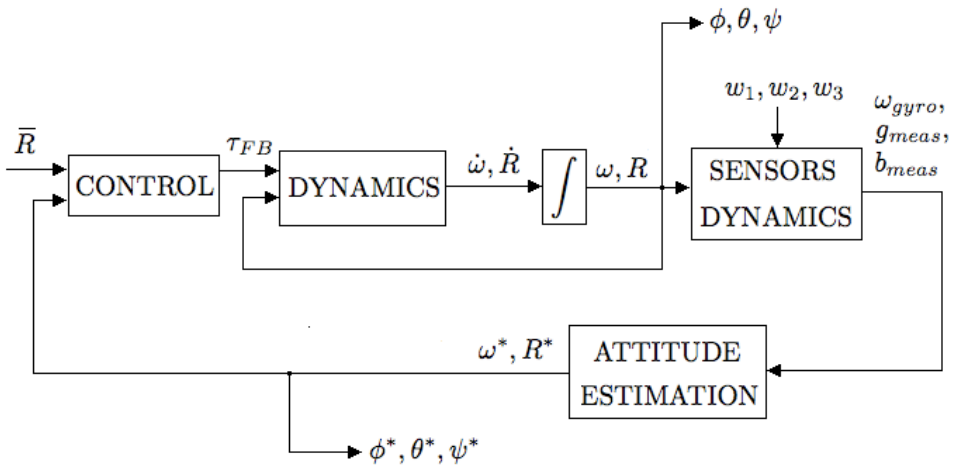

Figure 9: Schematic design of the control algorithm implementation.

Because $R^*(0)$ is chosen to be the identity matrix I, the estimation initially differ from the actual position, thus a transient in the attitude estimation is observed. Also, to simulate a linear acceleration of the body due for example to a transition from hovering to cruise, a $0.5g$ disturbance lasting $0.5s$ is introduced along the x-axis at time $t_1 = 2s$ (see Fig. 11), thus causing a temporary estimation error in R^* and therefore a displacement from the equilibrium position, which is eventually compensated for after the disturbance disappear.

6 Conclusion

In this work we presented a geometric (i.e. intrinsic and coordinate- free) approach to robust attitude estimation, derived from multiple and possibly redundant bio-inspired navigation sensors, for attitude stabilization of a micromechanical flying insect.

Such a multimodal sensor fusion was implemented by a dynamic observer, in particular a complementary filter is proposed which is specialized to the nonlinear structure of the Lie group of rigid body rotations.

[6]For the sake of simplicity the continuous time version is here presented; in fact a discretization of this algorithm is operated, using the Rodrigues' formula of Eqn. (9) to guarantee $R(t)$ and $R^*(t)$ not to drif from $SO(3)$

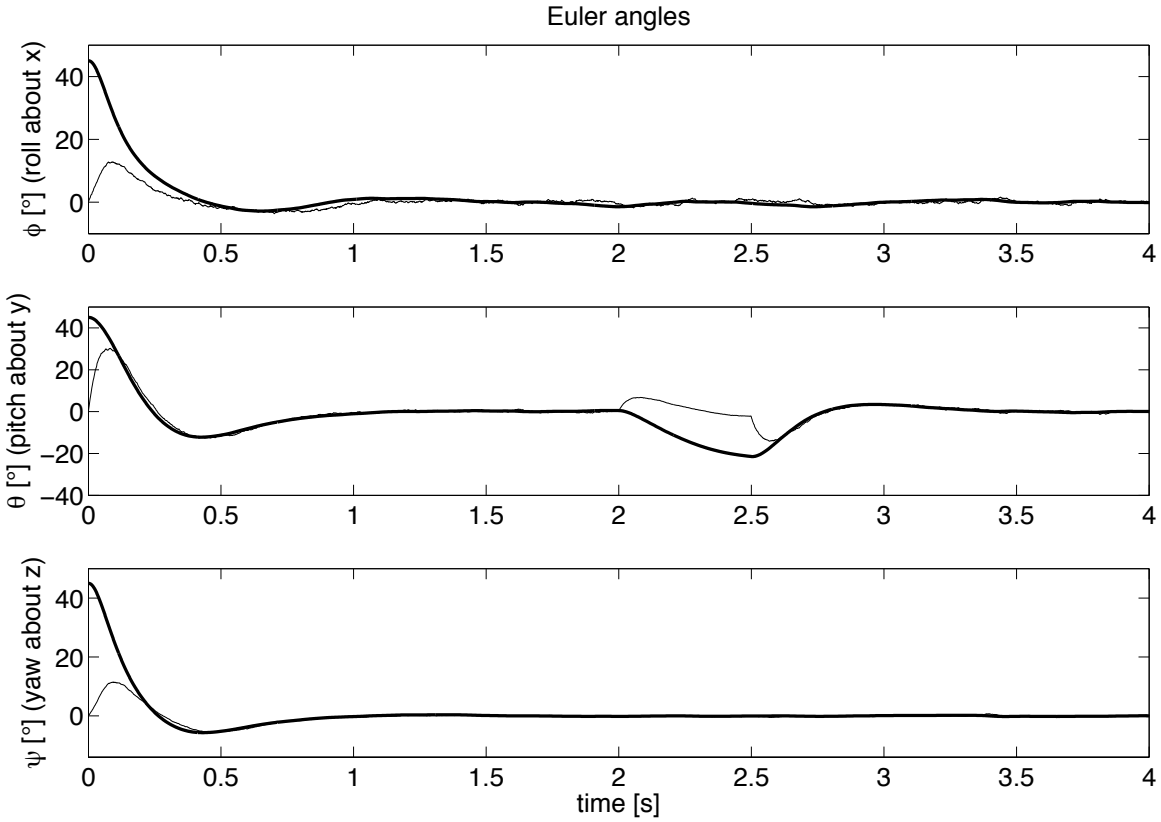

Figure 10: Actual Euler angles (thicker line), compared with their estimation (thinner line) in a $4s$ simulation.

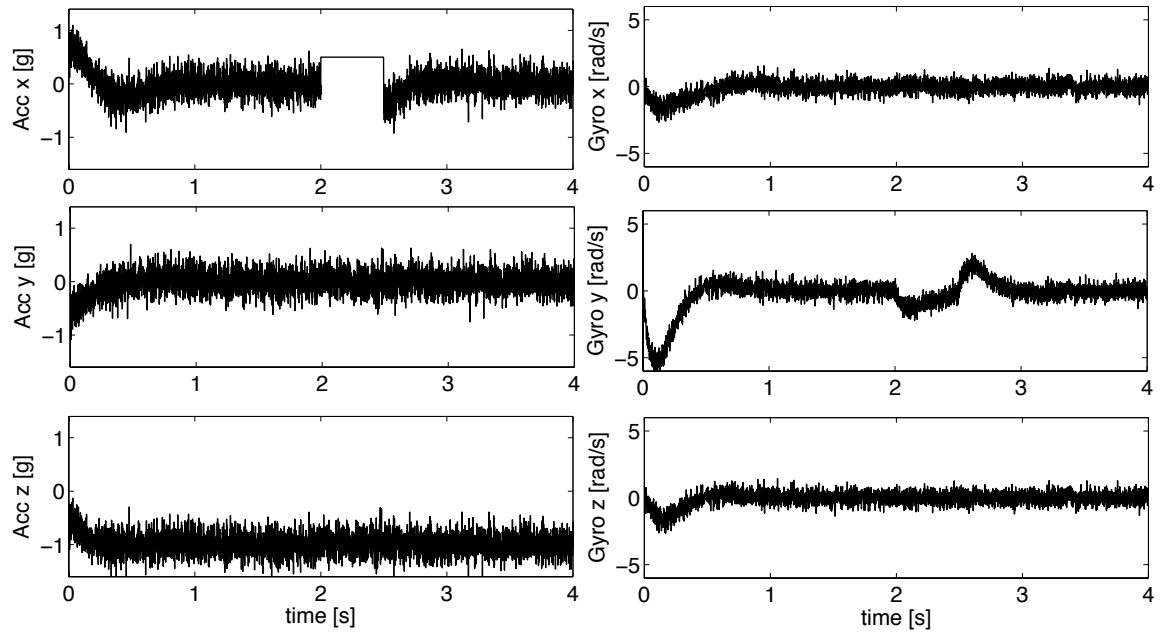

Figure 11: Data measured from the simulated accelerometers (on the left) and gyroscopes (on the right): a $0.5g$ disturbance is introduced in the accelerometer-x from $t_1 = 2s$ to $t_1 = 2.5s$.

The numerical implementation was also provided in the specific case of interest for inertial/magnetic navigation, i.e. when gravitometers, magnetometers and gyroscopes are available.

Performance of the proposed filter was experimentally tested. In particular, a 3-degree of freedom robotic flapper was used to generate a known trajectory and compare it with the estimated trajectory from the filter, showing good performance.

We then merged the proposed filter with state-feedback attitude control techniques which was proven to provide a globally stable control system for body attitude based on a generalized *separation principle* valid for Lie Groups. Moreover, the proposed controller does not depend on specific choice of coordinated, thus leading to easy and robust implementation on robotic flying insects.

As future work, theoretical performance properties of the proposed observer will be analyzed in presence of noisy data and disturbances(e.g. non- inertial accelerations, geomagnetic field distortion etc...). The filter will be also tested in more realistic conditions: miniaturized inertial/magnetic systems will be mounted onboard of small flying vehicles as well as biomimetic swimming robots.

APPENDIX

A Complementary Filtering on $SO(3)$

Consider $N \geq 2$ homogenous and time-invariant vector fields $\vec{v}_1, \vec{v}_2, \ldots, \vec{v}_N$ (e.g. the gravitational field, the geomagnetic field, the light direction etc...) and assume that at least two of them (e. g. $\vec{v}_1$ and $\vec{v}_2$, without loss of generality) are independent, which can be expressed in any coordinate frame as:

$$\vec{v}_1 \times \vec{v}_2 \neq 0 \tag{A-1}$$

Definition 1 *Given a rigid body, define a body frame $\mathcal{B}$ on it. Let the rigid body be at rest at some time t_0 and define thus a space frame $\mathcal{S}_0$ as the one coincident with the body frame $\mathcal{B}$ at time t_0. Let the constant vectors $v_{i0} = [v_{i0x}\ v_{i0y}\ v_{i0z}]^T$ represent the components of each vector field at time t_0 as measured by a set of sensors on the rigid body. At any time t, let $R(t) : \mathbb{R} \to SO(3)$ be a twice-differentiable function representing the orientation of the rigid body in 3D space with respect to the space frame $\mathcal{S}_0$, let $v_i = [v_{ix}\ v_{iy}\ v_{iz}]^T$ be the (time-variant) components of each field and let ω_{gyr} be readouts of the gyroscopes, both v_i and ω_{gyr} are referred to the (body) moving frame.*

Lemma 1 *The trajectory $R(t) \in SO(3)$, defined as in Definition 1, is reflected in the measurements of the gyroscopes and of the vector fields sensors and can be expressed as*

$$\begin{cases} \widehat{\omega}_{gyr} &= R^T \dot{R} = \widehat{\omega} \\ v_i &= R^T v_{0i} \end{cases} \tag{A-2}$$

Lemma 2 *Let $R(t) : \mathbb{R} \to SO(3)$ represent, as in Definition 1, the trajectory on $SO(3)$ of a rigid body embedding a set of gyroscopes and let the angular velocity ω of the rigid body be available, as in (A-2), via readings from such gyroscopes. Let $R^{*T}\dot{R}^* = \widehat{\omega}$ denote the dynamics of an estimator, then the tracking error*

$$E \triangleq R^T R^* \tag{A-3}$$

is such that $\|E(t)\|_{SO(3)} = constant$. In particular, the following identity holds:

$$\langle \langle \log(E), -E^T \widehat{\omega} E + \widehat{\omega} \rangle \rangle_{so(3)} = 0 \tag{A-4}$$

Theorem 1 *Let $R(t) : \mathbb{R} \to SO(3)$ represent the orientation of the rigid body as in Definition 1. Let $R^*(t)$ denote the estimate of $R(t)$ and let it be defined by the following observer:*

$$\begin{cases} \dot{R}^* &= R^* \widehat{\omega}^* \\ \omega^* &= \omega_{gyr} + \sum_{i=1}^{N} k_i (v_i \times v_i^*) \\ v_i^* &= R^{*T} v_{0i} \end{cases} \tag{A-5}$$

where $k_i > 0$ are the filter gains, ω_{gyr} and v_i represent the sensor readings as in (A-2).

The observer (A-5) asymptotically tracks $R(t)$ *for* almost *any initial condition* $R^*(0) \neq R(0)$ *and in particular:*

$$\lim_{t\to\infty} R^T(t)R^*(t) = I \tag{A-6}$$

B Separation Principle on $SO(3)$

Here, the Lemma presented in [32, Corollary 2] and proved in [33] for a general Lie group G, is restated for the specific case of interest $G = SO(3)$.

Consider the system

$$\begin{cases} \dot{R} = & R\,\omega \\ \dot{\omega} = & J^{-1}(J\omega \times \omega + \tau_{FB}(R,\omega)) + \psi(R,\omega,q) \end{cases} \tag{B-1}$$

with $(R,\widehat{\omega}) \in SO(3) \times so(3)$ and $q \in \mathbb{R}^n$ and $V = U(R) + \frac{1}{2}\langle\langle \widehat{\omega},\widehat{\omega}\rangle\rangle_{so(3)}$, where $U(R)$ is a smooth globally defined Morse function representing the potential energy of the system. Also consider the following assumptions.

Assumption A.1: *The point $(\bar{R},0)$ is an almost globally stable equilibrium point of (B-1) with $\psi \equiv 0$ and furthermore*

$$\langle\langle R^T \mathtt{grad}\, U,\widehat{\omega}\rangle\rangle_{so(3)} + \langle\langle J^{-1}\widehat{\tau}_{FB},\widehat{\omega}\rangle\rangle_{so(3)} \leq 0 \tag{B-2}$$

The condition (B-2) is satisfied by any simple mechanical system with potential energy $U(R)$ and Rayleigh-type dissipation. The equilibrium $(\bar{R},0)$ is an almost globally stable equilibrium if $\bar{R}$ is a unique minimum of $U(R)$.

Assumption A.2: *The function $q(t) \in \mathbb{R}^n$ satisfies*

$$\|q(t)\| \leq c\|q(0)\|e^{-\lambda t} \tag{B-3}$$

for some $c > 0$, $\lambda > 0$, and all $t > 0$.

Assumption A.3: *The interconnection term satisfies $\psi(R,\omega,0) \equiv 0$ and the linear growth conditions*

$$\|\psi\| \leq \gamma_1(\|q\|)\,\|\omega\| + \gamma_2(\|q\|) \tag{B-4}$$

for two $\mathcal{K}_\infty$ functions $\gamma_1(\cdot)$, $\gamma_2(\cdot)$.

Lemma 3 *If the Lie group G is compact and if Assumptions A.1-A.3 are satisfied, then the equilibrium $(\bar{R},0)$ of the system (B-1) is almost-globally stable. Convergence is asymptotic if the inequality in Assumption A.1 is strict.*

REFERENCES

[1] R.S. Fearing, K.H. Chiang, M.H. Dickinson, D.L. Pick, M. Sitti, and J. Yan. Transmission mechanism for a micromechanical flying insect, in *Proc of the IEEE International Conference on Robotics and Automation (ICRA)*, 2000.

[2] M.H. Dickinson, F.O. Lehnmann, and S.S. Sane. Wing rotation and the aerodynamic basis of insect flight. *Science*, **284**(5422):1954-1960, 1999.

[3] R.J. Wood. Design, fabrication, and analysis, of a 3DOF, 3cm flapping-wing MAV, in *Proc. of the IEEE/RSJ International Conference on Intelligent Robotics and Systems (IROS)*,San Diego, CA, USA, Oct 29 - Nov 2, 2007.

[4] R.J. Wood, The first takeoff of a biologically-inspired at-scale robotic insect , *IEEE Trans. on Robotics*, Vol.24, No. 2, pp. 341-347, April, 2008.

[5] G.K. Taylor. Mechanics and aerodynamics of insect flight control, in *Biological Review*, Vol. 76, No. 4, pp. 449-471, 2001

[6] P. Vela, K. Morgansen, and J.W. Burdick, Trajectory stabilization for a planar carangiform fish, in *Proc of the IEEE International Conference on Robotics and Automation (ICRA)*, Washington DC, U.S.A, May 2002.

[7] X. Deng and L. Schenato and W.C. Wu and S.S. Sastry, *Flapping Flight for Biomimetic Robotic Insects. Part I: System modeling*, IEEE Transactions on Robotics, Vol. 22, No. 4, pp. 789- 803, 2006.

[8] X. Deng and L. Schenato and S.S. Sastry, Flapping Flight for Biomimetic robotic Insects. Part II: Flight Control Design. In *IEEE Transactions on Robotics*, Vol. 22, No. 4, pp. 789- 803, 2006.

[9] L. Schenato and W.C. Wu and S.S. Sastry. Attitude Control for a Micromechanical Flying Insect Via Sensor Output Feedback, *IEEE Transactions on Robotics and Automation*, Vol. 20, pp. 93-106, 2004

[10] H. Rifai and N. Marchand and G. Poulin. Bounded attitude control of a biomimetic flapping robot, in *Proc. of the IEEE International Conf. on Robotics and Biomimetics (ROBIO)*, pp. 1-6, Sanya, China, Dec 2007.

[11] M. Epstein, S. Waydo, S.B. Fuller, W. Dickson, A. Straw, M.H. Dickinson, R.M. Murray, Biologically Inspired Feedback Design for Drosophila Flight, in *Proc. of the IEEE American Control Conference (ACC)*, pp. 3395-3401, 2007

[12] V. I. Arnold, *Mathematical Methods of Classical Mechanics*, 2 nd ed., Springer-Verlag, New York, 1989.

[13] R. M. Murray, Z. Li, and S. S. Sastry, *A Mathematical Introduction to Robotic Manipulation*, CRC, Boca Raton, FL, 1994.

[14] T. Frankel, *The Geometry of Physics: an Introduction*, Cambridge University Press, Cambridge, UK, 1997.

[15] S. S. Sastry, *Nonlinear Systems: Analysis, Stability and Control*, Springer, New York, 1999.

[16] F. Bullo and A. D. Lewis, *Geometric Control of Mechanical Systems*, Springer, 2005.

[17] F. Bullo and R. F. Murray *Proportional derivative (PD) Control on the Euclidean Group*, Technical report, California Institute of Technology, Anaheim, CA USA, 1995.

[18] S.P. Sane, *The aerodynamics of insect flight*, The Journal of Experimental Biology, Vol. 206, pp. 4191-4208, 2003.

[19] J. Chahl, *Bioinspired Engineering of Exploration Systems: A Horizon Sensor/Attitude Reference System Based on the Dragonfly Ocelli for Mars Exploration Applications*, Journal of Robotic Systems, Vol. 20, No. 1, pp. 35-42 2003.

[20] R. Hengstenberg, *Mechanosensory control of compensatory head roll during flight in the blowfly Calliphora erythrocephala*, Journal of Comparative Physiology A-Sensory Neural & Behavioral Physiology, Vol. 163, pp. 151-165, 1988.

[21] G. Nalbach, *The halteres of the blowfly C alliphora: I. Kinematics and dynamics*, Journal of Comparative Physiology A, Vol. 173, pp. 293-300, 1993.

[22] W. C. Wu, R. J. Wood and R. F. Fearing, *Halteres for the Micromechanical Flying Insect*, in Proc. of IEEE Intl. Conf. on Robotics and Automation (ICRA), pp. 60-65, 2002.

[23] M.H. Dickinson, *Linear and nonlinear encoding properties of an identified mechanoreceptor on the fly wing measured with mechanical noise stimuli*, The Journal of Experimental Biology, Vol. 151, pp. 219-244, 1990.

[24] H. Schuppe and R. Hengstenberg, *Optical properties of the ocelli of Calliphora erythrocephala and their role in the dorsal light response*, Journal of Comparative Biology A, Vol. 173, pp. 143-149,1993.

[25] W. Reichardt and M. Egelhaaf, *Properties of individual movement detectors as derived from behavioural experiments on the visual system of the fly*, in Biological Cybernetics, Vol. 58, No. 5, pp. 287-294, 1988.

[26] D. Lambrinos, H. Kobayashi, R. Pfeifer, M. Maris, T. Labhart, R. Wehner, *Adaptive Behavior An Autonomous Agent Navigating with a Polarized Light Compass*, Adaptive Behavior, Vol. 6, No. 1, pp. 131-161, 1997.

[27] E. Wajnberga and G. Cernicchiaroa and D. Acosta-Avalosb and L. J. El-Jaicka and D. M. S. Esquivel, *Induced remanent magnetization of social insects*, Journal of Magnetism and Magnetic Materials, Vol. 226-230, pp. 2040-2041, 2001.

[28] W. C. Wu, L. Schenato, R. J. Wood and R. F. Fearing, *Biomimetic Sensor Suite for Flight Control of MFI: Design and Experimental Results*, in Proc. of IEEE Intl. Conf. on Robotics and Automation (ICRA), pp. 1146-1151, 2003.

[29] R. G. Brown and P. Y. C. Hwang, "*Introduction to random signals and applied Kalman filtering*", New York: J. Wiley, 1992.

[30] F. Daum, *Nonlinear Filters: Beyond the Kalman Filter*, IEEE A&E Systems Magazine, Vol.20, No. 8, August 2005.

[31] D. Campolo, L. Schenato, L. Pin, X. Deng, E. Guglielmelli. Attitude Stabilization of Biologically Inspired Micromechanical Flying Insects. Part I: Attitude Estimation via Multimodal Sensor Fusion. to appear on *Advanced Robotics* (Special Issue on Biomimetic Robotics).

[32] D. H. S. Maithripala, J. M. Berg and W. P. Dayawansa, "*An Intrinsic Observer for a Class of Simple Mechanical Systems on a Lie Group*", SIAM Journ. Control Optim., Vol. 44, No. 5, pp. 1691-1711, Nov. 2005.

[33] D. H. S. Maithripala, J. M. Berg, and W. P. Dayawansa, *" Almost-Global Tracking of Simple Mechanical Systems on a General Class of Lie Groups"*, IEEE Trans. on Automatic Control, Vol. 51, No. 1, Jan. 2006.

[34] D. E. Koditschek, *The application of total energy as a Lyapunov function for mechanical control systems*, in J. E. Marsden, P. S. Krishnaprasad & J. C. Simo (eds), *Dynamics and Control of Multibody Systems*, Vol. 97, AMS, pp. 131-157, 1989.

[35] F. Bullo and R. M. Murray, *Tracking for Fully Actuated Mechanical Systems: a Geometric Framework*, Automatica, Vol. 35, No. 1, pp. 17-34 Jan. 1999.